PLANT SCIENCE

Brassinosteroid coordinates cell layer interactions in plants via cell wall and tissue mechanics

Robert Kelly-Bellow[1]*†, Karen Lee[1]†, Richard Kennaway[1], J. Elaine Barclay[1], Annabel Whibley[1], Claire Bushell[1], Jamie Spooner[1], Man Yu[1], Paul Brett[2], Baldeep Kular[2], Shujing Cheng[3], Jinfang Chu[3,4], Ting Xu[5], Brendan Lane[6], James Fitzsimons[7], Yongbiao Xue[5], Richard S. Smith[6]*, Christopher D. Whitewoods[1,7]*, Enrico Coen[1]*

Growth coordination between cell layers is essential for development of most multicellular organisms. Coordination may be mediated by molecular signaling and/or mechanical connectivity between cells, but how genes modify mechanical interactions between layers is unknown. Here we show that genes driving brassinosteroid synthesis promote growth of internal tissue, at least in part, by reducing mechanical epidermal constraint. We identified a brassinosteroid-deficient dwarf mutant in the aquatic plant *Utricularia gibba* with twisted internal tissue, likely caused by mechanical constraint from a slow-growing epidermis. We tested this hypothesis by showing that a brassinosteroid mutant in *Arabidopsis* enhances epidermal crack formation, indicative of increased tissue stress. We propose that by remodeling cell walls, brassinosteroids reduce epidermal constraint, showing how genes can control growth coordination between layers by means of mechanics.

Many multicellular organisms are formed from multiple cell layers, raising the question of how growth is coordinated between layers to produce an integrated final form. In plants, evidence from genetic chimeras and from layer-specific modification of gene function shows that genes active in one layer can act nonautonomously to influence growth in other layers (*1*–*4*). Nonautonomy could be explained through chemical signaling between layers and/or mechanical interactions.

Mechanics may act nonautonomously through the generation of tissue stresses (*5*), as demonstrated experimentally by Hofmeister more than 150 years ago (*6*). To understand the origin of tissue stresses, consider a cylindrical tissue in which cells are tightly stuck together, with all cells having the same size, turgor, wall material properties, and wall thickness (Fig. 1A). If cell walls are anisotropic, such that they yield more readily in the vertical orientation, the vertical component of turgor forces in each cell can cause stresses (highlighted for three cells with black double-headed arrows) that produce axial growth. There are no growth conflicts between cells. However, if the epidermal walls (Fig. 1B, purple) yield less to turgor (e.g., because they are thicker or less extensible than inner walls), an epidermal growth constraint is generated, and load is transferred from inner to outer walls. Each cell experiences mechanical stresses caused by the cell's own turgor (cell-autonomous stresses) and by mechanical effects from surrounding tissue (non–cell-autonomous stresses) (*7*) called tissue stresses (*5*). Whereas the cell-autonomous stress is always tensile, by our definition, tissue stresses can be tensile or compressive; epidermis is under tissue tension (Fig. 1B, divergent red arrows), whereas internal regions are under tissue compression (convergent blue arrows).

Tissue stresses can be revealed by immediate outward recurvature of median slices through internodes or by the formation of epidermal cracks when adhesion between cells is weakened (*6*, *8*, *9*). They can be quantified by stretching detached epidermal tissue to the point that its original length is restored (*10*, *11*). However, little is known about how tissue stresses are controlled genetically and thus the role they may play in non–cell-autonomous gene action. In this study, we addressed this problem through the analysis of dwarf mutants in the aquatic plant *Utricularia gibba* and the terrestrial plant *Arabidopsis thaliana*.

U. gibba dwarf has twisted internal tissue

U. gibba is a carnivorous plant with a spiral vegetative growing tip, comprising an apex that produces stolons bearing filiform leaves and traps (*12*) (Fig. 2A). The stolons and leaves have internal air spaces that allow the plant to float just below the water surface. To obtain developmental mutants in *U. gibba*, we carried out ethyl methanesulfonate mutagenesis. Obtaining large numbers of progeny proved difficult because of poor seed set and germination rates. Rather than mutagenizing seed, we therefore mutagenized small stolon explants and grew each on to flowering (see methods in the supplementary materials for details). M1 seed was collected from 441 explants and gave

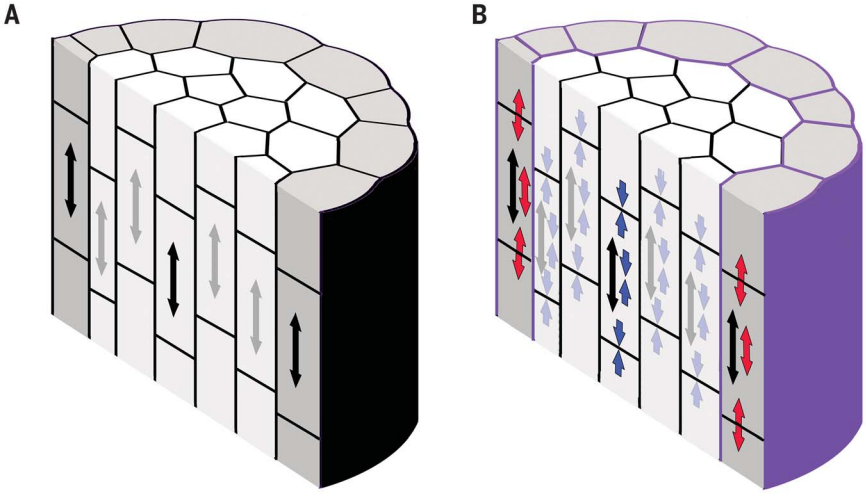

Fig. 1. Origin of tissue stresses. (**A**) Cross section of a stem, with epidermal cells in gray and cell walls in black. All cell walls have the same material properties. Vertical component of turgor forces autonomous to each cell causes stresses (highlighted for three cells with black double-headed arrows) that produce axial growth. There are no growth conflicts between cells. (**B**) If the epidermal walls (purple) yield less to turgor, an epidermal growth constraint is generated. Each cell now experiences two types of stress: cell-autonomous stress caused by the cell's own turgor (black double-headed arrows) and tissue stress caused by mechanical effects from surrounding tissue. Tissue stresses can be tensile (divergent red arrows) or compressive (convergent blue arrows).

[1]Department of Cell and Developmental Biology, John Innes Centre, Norwich NR4 7UH, UK. [2]Department of Biochemistry and Metabolism, John Innes Centre, Norwich NR4 7UH, UK. [3]National Centre for Plant Gene Research (Beijing), Institute of Genetics and Developmental Biology, Chinese Academy of Sciences, Beijing 100101, China. [4]College of Advanced Agricultural Sciences, University of Chinese Academy of Sciences, Beijing 100039, China. [5]State Key Laboratory of Plant Cell and Chromosome Engineering, Institute of Genetics and Developmental Biology, Chinese Academy of Sciences, Beijing 100101, China. [6]Department of Computational and Systems Biology, John Innes Centre, Norwich NR4 7UH, UK. [7]Sainsbury Laboratory, University of Cambridge, Cambridge CB2 1LR, UK.
***Corresponding author. Email: robert.bellow@jic.ac.uk (R.K.-B.); richard.smith@jic.ac.uk (R.S.S.); chris.whitewoods@slcu.cam.ac.uk (C.D.W.); enrico.coen@jic.ac.uk (E.C.)**
†These authors contributed equally to this work.

M2 phenotypes including altered traps, absent traps, reduced leaf and stolon growth, long flower spurs, spiky leaves, multiple traps on leaves, and fasciation. One M2 family contained two dwarf plants, and self-seed from a wild-type sib gave 37 wild-type, 9 dwarf, and 3 extreme-dwarf plants (Fig. 2, A to C), consistent with segregation of two recessive mutations: *dwarf* and *enhancer of dwarf*.

Both the dwarf and extreme-dwarf plants had short internodes, short leaves, and small traps (Fig. 2, A to D). To follow their development, we numbered internodes sequentially relative to the spiral apex, with internode 1 corresponding to the first clearly visible internode to emerge from the apex (fig. S1). Wild-type internode length increased until about internode 4, after which it plateaued to give a mature internode length of ~2 mm (Fig. 2E). By contrast, dwarf and extreme-dwarf plants exhibited very little growth after internode 1, generating mature internode lengths of ~0.7 and ~0.3 mm, respectively (Fig. 2E). Epidermal cells of mutant stolons were shorter and smaller than those of wild type (Fig. 2, F to J). Measurements of cell lengths parallel to the stolon axis indicated that 70% of the reduction in dwarf internode length was caused by reduced longitudinal growth after cell division arrest (fig. S2A). Further reduction in internode length in extreme dwarf was caused by reduced growth before division arrest. In addition to reduced internode length, both dwarf and extreme dwarf exhibited a significant increase in stolon circumference and number of epidermal cells in transverse sections compared with wild type, indicating increased radial and circumferential growth before division arrest (fig. S2, B and C).

We next determined the phenotype of internal tissues. Wild-type stolons had a cylindrical epidermis (Fig. 3C, purple) connected by five or six straight "blades" (cyan) to an axial cylinder of large cells (yellow) surrounding a vascular bundle (orange), with air spaces (magenta) between the blades (Fig. 3, A to C). Dwarf stolons had smaller air spaces, twisted blades, and a sinuous contorted vascular bundle (Fig. 3, D to F). Extreme-dwarf stolons had smaller air spaces and less-twisted vasculature than dwarf plants (Fig. 3, G to I). Both dwarf and extreme-dwarf plants sank in water, presumably because of their reduced air spaces.

The twisted internal tissue of the dwarf plants might be caused by a contorted pattern of early vascular and blade cell-type specification or by altered tissue growth after specification has occurred. To distinguish between these possibilities, we determined the developmental timing of the twisted phenotype in dwarf plants. Straight vasculature cell types surrounded by blade and air spaces were evident at internodes 0 in dwarf (Fig. 3J), as in wild type (fig. S3A). Twisted vascular tissue in dwarf plants was only observed from internode 4 onward (Fig. 3K, orange line). Contortions of the blade were evident in dwarf mutants earlier, at internode 1, as tissue strips running perpendicular to the vascular axis in longitudinal sections (Fig. 3J, blue arrow). These blade contortions were only seen after air spaces had formed. Thus, contortion and twisting of internal tissue in dwarf plants arose through altered growth after cell type specification and air space formation, leading to excess vascular length compared with epidermal length (fig. S2D). In extreme-dwarf plants, which showed little contortion, organized vasculature and surrounding tissue were evident in early internodes, but air spaces were not (fig. S3B).

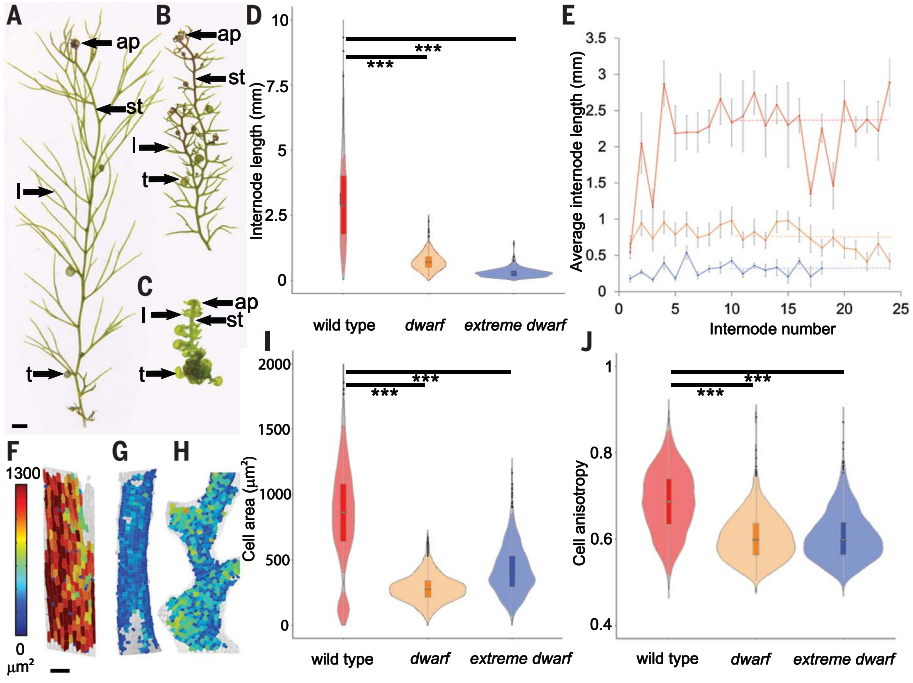

Fig. 2. External phenotype of *U. gibba* wild type and dwarf mutants. (**A** to **C**) *U. gibba* vegetative plants comprise a spiral apex (ap), filiform leaves (l), stolons (st), and traps (t). (A) Wild type. (B) Dwarf. (C) Extreme dwarf. Scale bar, 1 mm. (**D**) Violin plots of wild type [$\bar{x}$ = 3.07 mm ± 0.11 (SEM), n = 10], dwarf [$\bar{x}$ = 0.72 mm ± 0.02 (SEM), n = 10], and extreme dwarf [$\bar{x}$ = 0.29 mm ± 0.01 (SEM), n = 13] mature internode lengths from plants grown in continuous culture. Block indicates interquartile range, and horizontal line the mean. Both mutants have reduced lengths compared with wild type (***P < 0.001). (**E**) Internode lengths from growing explants of wild type (red), dwarf (orange) and extreme dwarf (blue) plotted against internode number. Dashed line shows mean from internode 10 onwards (n > 4 plants). (**F** to **H**) Cell areas in mature stolons of wild type (F), dwarf (G), and extreme dwarf (H), color coded according to the color scale shown at the left of (F). Scale bar, 100 μm. (**I** and **J**) Violin plots of cell area (I) and cell anisotropy [cell maximum length/(cell maximum length + cell minimum length)] (J) of mature stolons of wild type (n = 1817 cells from eight explants), dwarf (n = 2289 cells from five explants), and extreme dwarf (n = 1494 cells from four explants). Both mutants have significantly lower values than wild type.

Twisted dwarf phenotype explained by epidermal constraint

To evaluate hypotheses that might account for both the internal twisting and shortened internode length of *dwarf* mutants, we modeled tissue growth using continuum mechanics. For these purposes, we distinguished between two types of regional growth: specified and resultant (*13*). Specified growth corresponds to the growth driven by a cell's own turgor, in mechanical isolation from other cells. Resultant growth corresponds to the growth generated when tissue stresses, which act non–cell-autonomously, are also factored in. Computational models allow tissue stresses and resultant growth to be calculated from an input pattern of specified growth rates and orientations.

We modeled a small length of *U. gibba* stolon as a stiff cylindrical epidermal sheet connected by blades to an axial core (Fig. 4, A to C, and fig. S9, A and B). Specified growth was oriented parallel to an axial (initially vertical) polarity field (Fig. 4A, arrows). To reduce boundary effects, each stolon end was constrained to remain flat and horizontal.

If all regions had the same specified growth rate, the cylinder elongated without generation of tissue stresses or twisting of internal

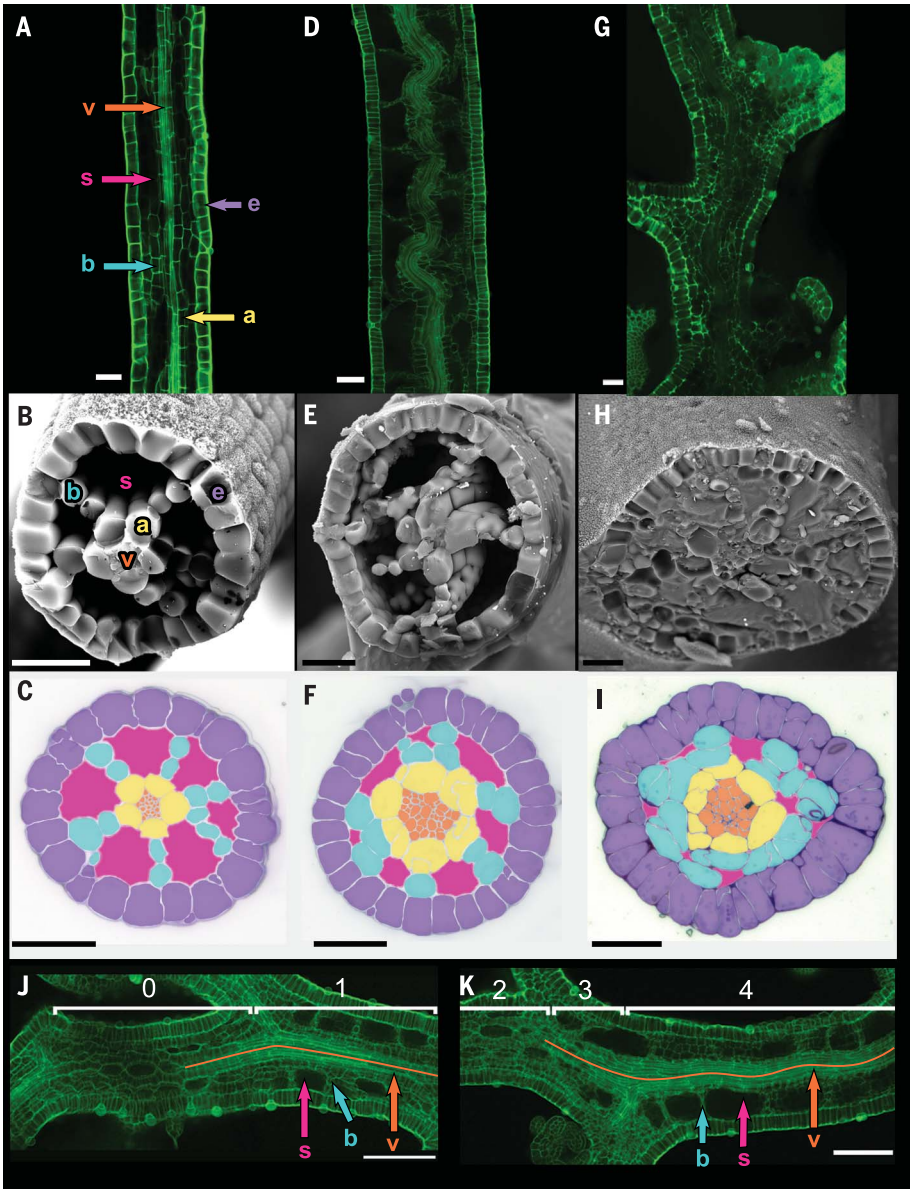

Fig. 3. Internal phenotype of *U. gibba* wild type and dwarf mutants. Wild type (**A** to **C**), dwarf (**D** to **F**), and extreme dwarf (**G** to **I**) longitudinal confocal sections [(A), (D), and (G)], freeze-fracture scanning electron microscopy [(B), (E), and (H)], and toluidine blue–stained transverse sections [(C), (F), and (I)]. Arrows and cells are color coded purple for epidermis (e), cyan for blades (b), magenta for air spaces (s), yellow for axial core (a), and orange for vasculature (v). Scale bars, 50 μm. (**J** and **K**) Confocal Z-slice of early dwarf internodes 0 to 4. Scale bars, 100 μm.

tissue (Fig. 4, D to F). If specified growth rate was set to zero in the epidermis, the epidermal constraint caused a dwarf phenotype (Fig. 4, G and H). Tissue tension was generated in the epidermis (Fig. 4I, red), and tissue compression was generated in the blades and core (Fig. 4, I and J, blue). The tissue tension caused the epidermis to grow to some extent, despite its specified growth rate being zero [compare epidermal resultant growth rate (Fig. 4K) with specified growth rate (Fig. 4G)]. Conversely, tissue compression in blades and core caused a lower resultant growth rate than specified (compare Fig. 4L with Fig. 4H), but higher than in the epidermis (zero). The tissue stresses also caused twisting of blades and core (Fig. 4, M to P, and movie S1). Thus, reduced specified growth rate in the epidermis captured both the dwarf phenotype and internal contortion.

Twisting of the axial core still occurred when blades were removed from a middle segment of the cylinder (fig. S4, A to F), showing that tissue compression could be transmitted to the core from above and below. No twisting occurred if the cylinder was solid (fig. S4, G to K), showing that air spaces were needed to accommodate buckling, and accounting for the reduced twisting observed in extreme dwarf plants. Restricting specified growth to the axial core led to a dwarf phenotype and a sinuous core but little twisting of the blades (fig. S4, L and M). Restricting specified growth to the blades gave a dwarf phenotype with twisted blades but little twisting of the core (fig. S4, N to P). Radial specified growth of the blades led to blade twisting, but cylinder elongation and axial core straightness were not affected (fig. S4, Q to V). Thus, both the dwarfism and internal axial and blade twisting could be most readily accounted for by reduced specified growth rate of the epidermis alone.

DWARF encodes a brassinosteroid biosynthetic enzyme

To understand the molecular basis of the *dwarf* mutant, we sequenced the wild-type progenitor and 33 wild-type, 10 dwarf, and 3 extreme-dwarf segregants. Only one single-nucleotide polymorphism (SNP) was absent from the progenitor, heterozygous or absent in wild-type segregants, and homozygous in all mutants, indicating that it was located in the *DWARF* gene. Extreme-dwarf plants carried four additional SNPs absent from the progenitor (table S1) that were candidate mutations in *ENHANCER OF DWARF*. Plants homozygous for *enhancer of dwarf* and heterozygous or homozygous for *DWARF* were scored as wild type, suggesting that the *enhancer of dwarf* mutation alone did not have a strong phenotypic effect. However, the mutation may have caused a subtle phenotype that we missed when initially scoring the families.

The *DWARF* SNP introduced an early stop codon in a gene encoding a cytochrome P450 90B1 enzyme, which catalyzes the C22-alpha-hydroxylation step in the brassinosteroid biosynthesis pathway (*14*). This gene is homologous to *DWARF4* (*DWF4*) in *Arabidopsis*, which affects cell area and cell anisotropy in a similar way to *U. gibba DWARF* (*15*, *16*). Brassinosteroid precursors after the C22-alpha-hydroxylation step were undetectable or at a low level in *dwarf* mutants, whereas a precursor before the step was present (fig. S5). Inhibiting brassinosteroid biosynthesis in wild type using brassinazole led to short stolons, smaller cells, and contorted vasculature, similar to *dwarf* mutants (fig. S6). Adding brassinosteroid, by growing mutants in epibrassinolide, rescued dwarf plants and partially rescued extreme dwarf plants (fig. S6). Thus, *DWARF* likely encodes a brassinosteroid biosynthesis gene.

To determine the timing of brassinosteroid action, we tracked dwarf stolons after treatment with epibrassinolide (Fig. 4S). Internodes that were not readily visible when the treatment began, because they were concealed

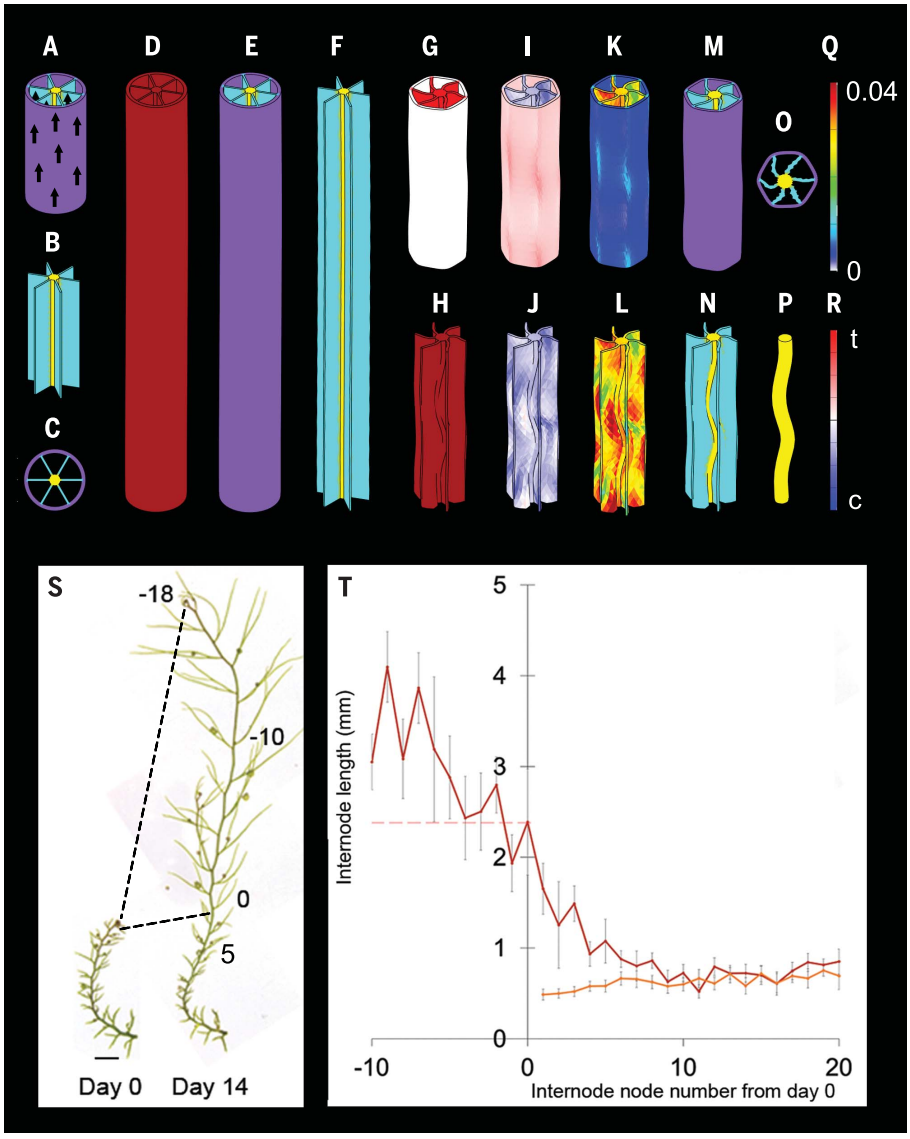

Fig. 4. Simulations of *U. gibba* wild type and dwarf mutant and timing of brassinosteroid action. (**A**) Initial state for wild-type and dwarf mutant models [epidermis (purple), blades (cyan), and axial core (yellow)]. Arrows indicate polarity. (**B**) Initial state without epidermis. (**C**) Transverse slice of (A). (**D**) Final state of wild-type simulation, color coded for specified growth rate, which is uniformly high. (**E**) Same as (D), but color coded for tissue type. (**F**) Same as (E), with epidermis removed. (**G**) Final state for simulation of dwarf mutant, color coded for specified growth rate, which is excluded from the epidermis and gives reduced elongation. (**I**) Same as (G), but color coded for tissue stresses. (**K**) Same as (G), but color coded for resultant growth rate. (**M**) Same as (G), but color coded for tissue type. (**H**, **J**, **L**, and **N**) Same as (G), (I), (K), and (M), respectively, but with epidermis clipped away. (**O**) Transverse slice of (M). (**P**) Same as (M), but showing the axial core only. (**Q**) Color scale for specified and resultant growth rates, in strain per time step of simulation. (**R**) Color scale for tissue stresses, with red indicating tension (t) and blue indicating compression (c). (**S**) A dwarf explant imaged on days 0 and 14 after treatment with 0.01 μM epibrassinolide. Internode numbers labeled on day 14. Scale bar, 5 mm. (**T**) Average internode lengths of dwarf explants before treatment (day 0, solid orange line) and at 14 days (day 14, solid brown line) ($n \geq 10$ explants). Day 14 internode −10 to 0 lengths were not significantly different from the mean of Fig. 2E (red dashed line). Error bars show SEM.

within the spiral vegetative shoot tip or had not yet initiated, were assigned consecutive negative numbers, starting from 0. These internodes grew to a length similar to those of mature wild type (Fig. 4T). Internodes 1 to 5 also showed a significant length increase in response to treatment ($P < 0.05$), with the magnitude of the increase declining with internode number. Thus, brassinosteroid likely acts from around internode 0, when cell division is nearing arrest, until around internode 5, by which stage cell elongation has arrested in wild type. However, we cannot rule out the possibility that internodes above 5 are impermeable to exogenous brassinosteroid.

Arabidopsis brassinosteroid mutant has elevated tissue stresses

Our experimental and modeling results indicate that brassinosteroid promotes *U. gibba* stolon growth starting just before cell division arrest by counteracting an epidermal constraint, thus reducing tissue stresses. If generally applicable, this hypothesis predicts that *Arabidopsis dwf4* mutants should also exhibit elevated tissue stresses. However, the effect of these stresses might be masked because *Arabidopsis* stems are solid and therefore lack air spaces to accommodate buckling (fig. S4, G to K). To determine whether tissue stresses are enhanced in *dwf4* mutants, we therefore exploited the *quasimodo2-1* (*qua2-1*) mutation, which weakens cell-cell adhesion (*17*). As illustrated in Fig. 1B (red arrows), tissue stresses generated a force that acts to pull epidermal cells apart. In wild-type *Arabidopsis*, cell-cell adhesion is strong enough to resist this force, but in *qua2-1* mutants, epidermal cracks are observed between cells in dark-grown hypocotyls, confirming that epidermal tissue tension is present (*9*, *18*). If brassinosteroid normally acts to reduce tissue tension, cracks are predicted to be exacerbated in *qua2-1 dwf4* double mutants, or in *qua2-1* mutants treated with a brassinosteroid inhibitor.

To test these predictions, we intercrossed *dwf4* and *qua2-1* mutant lines. About 1/16 (58/885) of the F2 dark-grown seedlings exhibited a distinctive novel phenotype: Hypocotyls were dwarf and seemed devoid of epidermis (Fig. 5, A and B), unlike *qua2-1* single mutants, which showed small epidermal cracks at a similar stage (Fig. 5C). To clarify the developmental origin of the double-mutant phenotype, we imaged seedlings at different days after germination. Seedlings of *dwf4 qua2-1* were indistinguishable from *dwf4* seedlings until ~3 days after stratification, when wide cracks appeared in the double mutant (Fig. 5D). These cracks were much larger than those observed in *qua2-1* single mutants at the same stage (Fig. 5E). By 5 days after stratification, the cracks in *dwf4 qua2-1* had enlarged to the extent that much of the epidermis was no longer evident (Fig. 5B). Crack formation was also enhanced when *qua2-1* single mutants were grown in the presence of a brassinosteroid inhibitor, brassinazole (Fig. 5, F to H). These results thus support the hypothesis that brassinosteroid promotes stem growth by counteracting an epidermal constraint.

To further validate this interpretation, we modeled the growth of a solid cylinder with a stiff epidermis in which cracks can form when tension exceeds a threshold value. Uniform specified growth rate gave elongation without

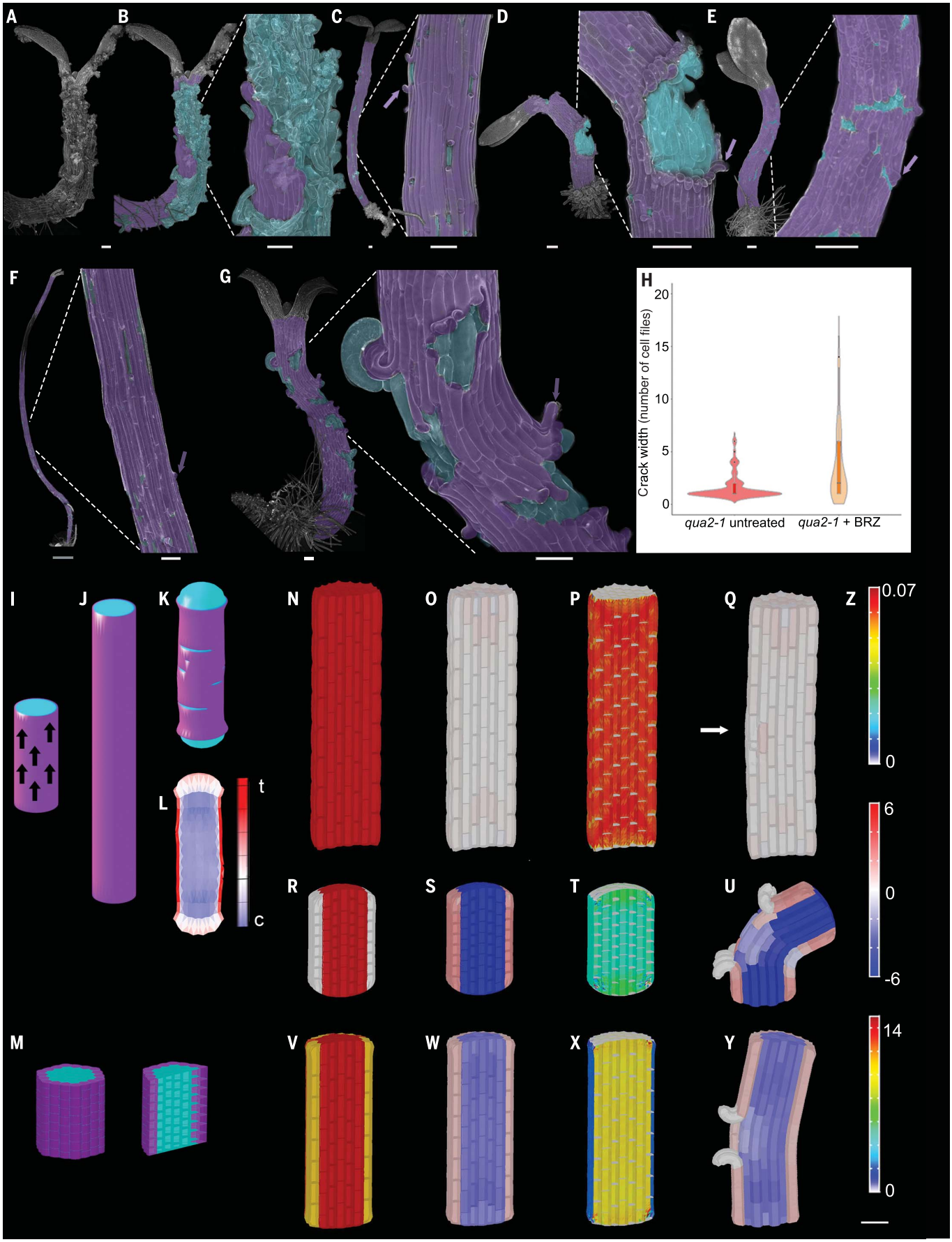

Fig. 5. Effect of reduced brassinosteroid on epidermal cracks in *Arabidopsis qua2-1* and explanatory computational models. (**A** to **C**) Confocal images 5 days after stratification. (A) *qua2-1 dwf4* double mutant. (B) *qua2-1* dwf4 shown in (A), with cells artificially colored for clarity (purple indicates epidermal cells, and cyan indicates interior cells). It is possible that the cyan-colored cells include some disorganized epidermal cells. Close-up shown on the right. (C) *qua2-1* single mutant with a close up of a region with cracks. (**D** and **E**) Confocal images 3 days after stratification. (D) *qua2-1 dwf4* double mutant. (E) *qua2-1* single mutant. Scale bars, 100 μm. Purple arrows highlight curled free ends of epidermal cells. (**F** to **H**) Phenotypes of *qua2-1 Arabidopsis* hypocotyls without or with treatment with brassinosteroid inhibitor [1 μM brassinazole (BRZ)]. [(F) and (G)] Confocal images of seedlings after 9 days growth in the dark. (F) *qua2-1* with close up of a region with cracks selected for magnification. (G) *qua2-1* grown on 1 μM BRZ with close up. Curved cells at crack boundaries are indicated with an arrow. Epidermal cells are in purple, internal cells are in cyan. Scale bars, 100 μm except in (F) (gray scale bar), which is 1000 μm. (H) Violin plots of crack widths measured by number of cells. Mean crack width covers more cell files in *qua2-1* + BRZ [$\bar{x}$ = 4.089 ± 0.38 (SEM)] than *qua2-1* untreated [$\bar{x}$ = 1.611 ± 0.14 (SEM)], but not significantly more (P = 0.0531, untreated hypocotyls n = 74 cracks from two plants, BRZ-treated hypocotyls n = 83 cracks from six plants). (**I** to **L**) Tissue-level computer simulations. (I) Initial state, with epidermis in purple and inner regions in cyan. Arrows indicate polarity. (J) Final state with all regions having the same specified growth parallel to polarity, leading to elongation without epidermal cracking. (K) Final state with reduced specified growth in the epidermis leads to a shorter cylinder and epidermal cracks. (L) Longitudinal section through (K), showing longitudinal tissue tension (t) in red and compression (c) in blue. (**M** to **Z**) Cellular-level computer simulations. (M) Initial state, with outer epidermal wall in dark purple, epidermis in purple, and inner tissue in cyan. [(N) to (Y)] Final state. [(N) to (Q)] All cell walls have the same thickness and material properties. [(R) to (U)] Outer epidermal wall is 10 times thicker. [(V) to (Y)] Outer wall is 10 times thicker, with higher extensibility and reduced yield threshold. [(Q), (U), and (Y)] Epidermal fracture introduced at an early stage. White arrow in (Q) indicates position of fracture. Fracture is two cells wide for (Q) and (U) and eight cells wide for (Y). [(N), (R), and (V)] Specified growth rate. [(O), (S), (W), (Q), (U), and (Y)] Tissue stresses. [(P), (T), and (X)] Resultant longitudinal wall stresses. (Z) Color scales. (Top) Specified growth rate (7% per time step). (Middle) Tissue stresses (*23*). (Bottom) Longitudinal wall stresses (*23*). Scale bar, 50 μm.

tissue stresses or cracks (Fig. 5, I and J), whereas low epidermal specified growth led to reduced elongation, elevated tissue stresses, and crack formation (Fig. 5, K and L).

Release from epidermal constraint by wall remodeling

The above results raise the question of how brassinosteroid reduces epidermal constraint. The most obvious source of epidermal constraint is the thick outer wall of the epidermal cells (*6*). A constraining outer wall is also consistent with the concave shape of the outer wall in epidermal cells released by crack formation (Fig. 5, C to E, purple arrows). Outer epidermal walls of *U. gibba dwarf* stolons were about two to three times thicker than inner walls at internode 1 (fig. S7, D and F), by which time growth had ceased (Fig. 2E). Outer epidermal walls of *A. thaliana dwf4* dark-grown hypocotyls were ~20 times thicker than inner walls at 4 days after stratification (fig. S7, C and E), by which time growth had largely ceased (fig. S8). Similar wall thicknesses were observed for wild types at comparable stages (fig. S7, A, B, E, and F), even though growth continued afterwards, suggesting that brassinosteroid does not reduce epidermal constraint primarily by altering wall thickness.

A possible mechanism for reduction of epidermal constraint is wall loosening. Brassinosteroids promote hypocotyl elongation within 6 hours of application through increased wall relaxation properties (i.e., wall loosening) (*19*, *20*), possibly through phosphorylation of plasma membrane proton adenosine triphosphatase (*21*). To explore the possible contribution of wall loosening, we modeled hypocotyl tissue growth at the cellular level. A segment of hypocotyl was modeled as a vertical cylinder of tightly attached cells of similar size and under the same turgor (Fig. 5M). Wall growth by means of creep (*22*) was simulated by converting a proportion of reversible elastic wall strain, above a yield threshold, into irreversible strain at each time step. The proportion corresponded to the extensibility of the wall. Walls were seven times stiffer (a sevenfold larger Young's modulus) in the transverse compared with longitudinal orientation, leading to vertical specified growth.

If all cell walls had the same material properties, the cylinder elongated with uniform specified growth rates (Fig. 5N), low tissue stresses (Fig. 5O), and uniform longitudinal wall stresses (Fig. 5P). Introducing an epidermal fracture caused rounding of the cell ends but did not cause further cell separation (Fig. 5Q, arrow indicates the position of fracture). Setting the outer epidermal wall to be 10 times thicker than the inner walls lowered the epidermal specified growth rate (Fig. 5R). The growth constraint generated longitudinal epidermal tissue tension and internal tissue compression (Fig. 5S). Resultant longitudinal wall stresses were uniform but lower than if all cell walls had the same material properties (compare Fig. 5T with Fig. 5P). The cylinder therefore grew less, capturing the *dwf4* phenotype. Introducing a wide epidermal fracture (eight cells wide) released epidermal cell ends to peel back (Fig. 5U and movie S2), capturing the *dwf4 qua2-1* phenotype (Fig. 5D).

To simulate wild type, the thick outer wall was loosened by increasing its extensibility and reducing its yield threshold. This modification increased the epidermal specified growth rate (compare Fig. 5V with Fig. 5R), lowered tissue stresses (compare Fig. 5W with Fig. 5S), and raised longitudinal wall stresses of internal tissue (compare Fig. 5X with Fig. 5T). The cylinder therefore elongated more than in the *dwf4* simulation, capturing the wild-type phenotype. Introducing a narrow epidermal fracture (two cells wide) led to released epidermal cell ends peeling back (they curve because the thick outer wall grows more slowly) (Fig. 5Y), capturing the *qua2-1* phenotype (Fig. 5C). Thus, brassinosteroid likely acts, at least in part, by loosening of the thick outer wall, counteracting the epidermal constraint.

In addition to wall thickness, epidermal constraint may be further enhanced by the orientation of microfibrils, which are less transverse in outer than in inner walls for wild-type *Arabidopsis* hypocotyls (*23*). Brassinosteroid treatment can cause microtubules of the outer epidermal plasma membrane to orient more transversely (*24*, *25*). Thus, brassinosteroid may reduce epidermal constraint by remodeling the thick outer wall in two ways: wall loosening and reducing the proportion of longitudinally oriented microfibrils. Such an effect on microfibril orientation might explain why *Utricularia dwarf* mutants have wider stolons (fig. S2, B and C). The differential properties of the outer epidermal wall (e.g., thickness, extensibility, microfibril orientation) may depend on cell polarity factors that confer differences between outer and inner cell faces (*26*–*28*). Brassinosteroids may also reduce epidermal constraint by increasing turgor in epidermal cells, although there is currently no experimental evidence to support this possibility.

Conclusions

When brassinosteroid synthesis or perception genes are expressed only in the epidermal cell layer of *Arabidopsis* brassinosteroid mutants, a near–wild-type phenotype is generated, even though these genes are normally expressed in both epidermis and ground tissue (*4*, *29*). Our results indicate that this nonautonomous effect of epidermal brassinosteroid gene expression on resultant growth of internal tissue involves release of internal tissue from epidermal mechanical constraint, although this does not preclude additional contributions from molecular signaling. Mechanical interactions

between cell layers also play a role in animal development, such as formation of crocodile skin cracks (*30*) and intestinal villi (*31*). Here we show how genes may modify tissue layer interactions by changing cellular growth properties and thus tissue stresses. Gene activity may therefore have coordinated effects on tissue development not only via molecular signaling but also via mechanics.

REFERENCES AND NOTES

1. S. Hake, B. R. Char, *Genes Dev.* **11**, 1087–1097 (1997).
2. M. H. Frank, D. H. Chitwood, *Dev. Biol.* **419**, 41–53 (2016).
3. R. A. Tilney-Bassett, *Plant Chimeras* (Edward Arnold Publishers Ltd., 1986).
4. S. Savaldi-Goldstein, C. Peto, J. Chory, *Nature* **446**, 199–202 (2007).
5. Z. Hejnowicz, A. Sievers, *J. Exp. Bot.* **46**, 1035–1043 (1995).
6. U. Kutschera, K. J. Niklas, *J. Plant Physiol.* **164**, 1395–1409 (2007).
7. F. Boudon *et al*., *PLOS Comput. Biol.* **11**, e1003950 (2015).
8. W. S. Peters, A. D. Tomos, *Ann. Bot.* **77**, 657–665 (1996).
9. S. Verger, Y. Long, A. Boudaoud, O. Hamant, *eLife* **7**, e34460 (2018).
10. Z. Hejnowicz, A. Sievers, *J. Exp. Bot.* **46**, 1045–1053 (1995).
11. U. Kutschera, *J. Plant Physiol.* **138**, 460–465 (1991).
12. P. Taylor, *The Genus* Utricularia*: A Taxonomic Monograph* (Royal Botanic Gardens, 1989).
13. E. Coen, R. Kennaway, C. Whitewoods, *Development* **144**, 4203–4213 (2017).
14. S. Fujioka *et al*., *Biosci. Biotechnol. Biochem.* **59**, 1543–1547 (1995).
15. R. Azpiroz, Y. Wu, J. C. LoCascio, K. A. Feldmann, *Plant Cell* **10**, 219–230 (1998).
16. S. Choe *et al*., *Plant Cell* **10**, 231–243 (1998).
17. S. Verger, S. Chabout, E. Gineau, G. Mouille, *Development* **143**, 2536–2540 (2016).
18. G. Mouille *et al*., *Plant J.* **50**, 605–614 (2007).
19. D. M. Zurek, D. L. Rayle, T. C. McMorris, S. D. Clouse, *Plant Physiol.* **104**, 505–513 (1994).
20. T. W. Wang, D. J. Cosgrove, R. N. Arteca, *Plant Physiol.* **101**, 965–968 (1993).
21. A. Minami, K. Takahashi, S. I. Inoue, Y. Tada, T. Kinoshita, *Plant Cell Physiol.* **60**, 935–944 (2019).
22. E. Coen, D. J. Cosgrove, *Science* **379**, eade8055 (2023).
23. E. F. Crowell *et al*., *Plant Cell* **23**, 2592–2605 (2011).
24. X. Wang *et al*., *Plant Cell* **24**, 4012–4025 (2012).
25. M. Catterou *et al*., *Planta* **212**, 673–683 (2001).
26. J. Takano *et al*., *Proc. Natl. Acad. Sci. U.S.A.* **107**, 5220–5225 (2010).
27. L. Łangowski, K. Růzicka, S. Naramoto, J. Kleine-Vehn, J. Friml, *Curr. Biol.* **20**, 904–908 (2010).
28. V. Gorelova, J. Sprakel, D. Weijers, *Nat. Plants* **7**, 1548–1559 (2021).
29. D. M. Friedrichsen, C. A. Joazeiro, J. Li, T. Hunter, J. Chory, *Plant Physiol.* **123**, 1247–1256 (2000).
30. M. C. Milinkovitch *et al*., *Science* **339**, 78–81 (2013).
31. A. E. Shyer *et al*., *Science* **342**, 212–218 (2013).
32. R. Kennaway, JIC-Enrico-Coen/Cell_Layer_Interactions_2023: GFtbox_Cell_Layer_Interactions_2023 (v1.0.1), Zenodo (2023); https://doi.org/10.5281/zenodo.7913146.

ACKNOWLEDGMENTS

We thank B. and P. Steward at The Fly Trap Plants and T. Bailey from the Carnivorous Plant Society for plants, seeds, and advice. We thank M. Majda for *qua2-1* seeds, E. Wegel and S. Lopez of John Innes Centre (JIC) Bioimaging for help with light microscopy, R. Wightman for help with freeze-fracture scanning electron microscopy, L. Perkins and the JIC horticulture team for large-scale *U. gibba* cultivation, G. Mosca for MorphoMechanX, and D. Bradley for critical reading of the manuscript. **Funding:** This work was supported by a European Research Council grant (323028-CarnoMorph) and Biotechnology and Biological Sciences Research Council grants (BBS/E/J/000PR9787, BB/M023117/1, BB/L008920/1, and BB/X01102X/1) awarded to E.C. **Author contributions:** Biological experiments, data analysis, and conceptualization: R.K.-B., K.L., J.E.B., M.Y., P.B., B.K., S.C., J.C., T.X., B.L., J.F., Y.X., R.S., and C.D.W. Computational modeling: R.K., R.S.S., and E.C. Software development: R.K. and R.S.S., Development of *U. gibba* resources: K.L., C.B., J.S., M.Y., and C.D.W. Bioinformatic analysis: R.K.-B. and A.W. Supervision, funding acquisition, and conceptualization: E.C. **Competing interests:** The authors declare that they have no competing interests. **Data and materials availability:** All data are available in the manuscript or the supplementary materials or are deposited at Zenodo (*32*).

SUPPLEMENTARY MATERIALS

science.org/doi/10.1126/science.adf0752
Materials and Methods
Supplementary Text
Figs. S1 to S9
Tables S1 and S2
References (*33*–*53*)
MDAR Reproducibility Checklist
Movies S1 and S2

View/request a protocol for this paper from *Bio-protocol*.

Submitted 5 October 2022; accepted 18 May 2023
10.1126/science.adf0752

Brassinosteroid coordinates cell layer interactions in plants via cell wall and tissue mechanics

Robert Kelly-Bellow, Karen Lee, Richard Kennaway, J. Elaine Barclay, Annabel Whibley, Claire Bushell, Jamie Spooner, Man Yu, Paul Brett, Baldeep Kular, Shujing Cheng, Jinfang Chu, Ting Xu, Brendan Lane, James Fitzsimons, Yongbiao Xue, Richard S. Smith, Christopher D. Whitewoods, and Enrico Coen

Science, **380** (6651), .
DOI: 10.1126/science.adf0752

Editor's summary

Cell layers can slip, slide, and fold in among one another during development to generate the complex forms of the biological world. Studying a small aquatic carnivorous plant as well as the land-locked mustard plant *Arabidopsis*, Kelly-Bellow *et al*. built a connection from genes driving a hormone's biosynthesis to the curved shapes of the mature plants. The plant hormone brassinosteroid reduces mechanical constraints imposed by the plant's epidermis, thus allowing internal cell layers to drive the formation of new shapes with development. —Pamela J. Hines